Available online at www.sciencedirect.com
SCIENCE DIRECT®
Journal of Organometallic Chemistry 690 (2005) 338–347
Journal of Organometallic Chemistry
www.elsevier.com/locate/jorganchem

Theoretical studies on the ground states in $M(terpyridine)_2^{2+}$ and $M(n\text{-butyl-phenylterpyridine})_2^{2+}$ (M = Fe, Ru, Os) and excited states in $Ru(terpyridine)_2^{2+}$ using density functional theory

Xin Zhou [a,*], Ai-Min Ren [a], Ji-Kang Feng [a,b]

[a] State Key Laboratory of Theoretical and Computational Chemistry, Institute of Theoretical Chemistry, Changchun, PR China
[b] College of Chemistry, Jilin University, Changchun 130023, PR China

Received 12 May 2004; accepted 17 September 2004

Abstract

We present a comparative study using density functional theory on the molecular structure, electronic structure and relative properties of $M(terpyridine)_2^{2+}$ ($M(tpy)_2^{2+}$) and $M(n\text{-butyl-phenylterpyridine})_2^{2+}$ ($M(B\text{-}ptpy)_2^{2+}$) (M = Fe, Ru, Os). The trends of the center ionic effects and the introduction of electron-donating groups on the electronic structure and chemical stabilities have been investigated in detail. The results show that, for $Ru(tpy)_2^{2+}$ and $Os(tpy)_2^{2+}$, the lowest energy transition are assigned as the singlet metal-to-ligand charge transfer (MLCT). For $Fe(tpy)_2^{2+}$, the lowest energy transition corresponds to the intraligand π–π* character. As the case of $M(B\text{-}ptpy)_2^{2+}$ (M = Fe, Ru, Os), the lowest energy transitions can be assigned as mixed metal/ligand-to-ligand charge transfer. The time dependent density functional (TDDFT) method is applied to calculate the singlet and triplet electronic states of $M(tpy)_2^{2+}$ (M = Fe, Ru, Os) based on the ground-state geometry. The three absorption bands observed experimentally for $Ru(tpy)_2^{2+}$ are well reproduced by the TDDFT technique. Some insights on the difference observed for these complexes in changing the central metal atom are given. The luminescence for $Ru(tpy)_2^{2+}$ originates from the lowest triplet excited states and is assigned to the MLCT character.

Keywords: Terpyridine; Density functional theory; Electronic structure

1. Introduction

Polypyridine complexes of transition metals as photosensitizers in model systems play important roles in fields relative to solar energy conversion, the storage of light and electronic information [1–5]. 2, 2′-bipyridine (bpy) complexes of metal, $M(bpy)_3^{2+}$ (M = Ru, Os) have been ones of the most studied metal-containing species in the last two decades [6,7]. But only a few photophysical reports have been devoted to terpyridine (tpy) $M(tpy)_2^{2+}$ analogs, because $M(tpy)_2^{2+}$ exhibits less favorable photophysical properties (lack of luminescence and a very short excited-state life time at room temperature) than $M(bpy)_3^{2+}$. The structures of $M(tpy)_2^{2+}$, however, are much more advantages over that of $M(bpy)_3^{2+}$: first, $M(tpy)_2^{2+}$ complexes are achiral, contrary to mixtures of *facial* and *meridional* isomerisms and two enantiomers; second, two substituents on $M(bpy)_3^{2+}$ complexes can give rise to triads with *cis*-type geometrical arrangements, without possibility of control, whereas substituents in the 4′-positions of $M(tpy)_2^{2+}$ lead

* Corresponding author. Tel.: +864318499856; fax: +86431894 5942.
E-mail address: kabinzx@hotmail.com (X. Zhou).

0022-328X/$ - see front matter © 2004 Elsevier B.V. All rights reserved.
doi:10.1016/j.jorganchem.2004.09.042

to triads where the two substituents lie in opposite directions with respect to the photosensitizer [8].

As for $Ru(tpy)_2^{2+}$, the experimental results show that the very intense bands in the UV-region are assigned to ligand-centered π–π* transition. The relatively intense and broad absorption band in the visible region is due to metal-to-ligand charge transfer (MLCT). At 77 K, $Ru(tpy)_2^{2+}$ exhibits a strong long-lived luminescence characteristic of a triplet MLCT (^{3}MLCT) level [9]. Compared with $Ru(tpy)_2^{2+}$, $Os(tpy)_2^{2+}$ complex exhibits a quite intense spin-forbidden MLCT band centered at 657 nm. The absorption maximum of the spin-allowed MLCT band in the visible region for $Os(tpy)_2^{2+}$ lies at the same wavelength as that of $Ru(tpy)_2^{2+}$ (476 nm) [10]. As for the metal compound of the same family $Fe(tpy)_2^{2+}$, no emission was observed and an excited state with 2.5 ns lifetime was obtained in aqueous solution at room temperature and was regarded as having metal-center orbital nature due to the weak ligand field of Fe(II) [11].

In contrast to the numerous experimental studies, few theoretical investigations are available on this topic despite the potential interest of an advanced quantum chemical approach for a better understanding of key issues, such as the nature of both the ground and the excited states involved in the absorption and emission. More than 10 years ago, Amouyal et al. [12] theoretically carried out molecular orbital studies of metal complexes M(R-phenylterpyridine)$_2^{2+}$ (M = Fe(II), Ru(II), Os(II), R = H, CH_3, OH, OCH_3 and Cl) using Pariser–Parr–Pople method and extended Hückel theory. The calculated results indicate the low luminescence quantum yield at room temperature is due to low-energy intramolecular vibrations of the nonrigid complex and not to the coupling with d states.

The main difficulties against liable computational approach are related to the large size of the ligands and the significant role of correlation and relativistic effects. In recent years, density functional theory (DFT) have received large acceptance for evaluating a variety of ground-state properties of organometallic and inorganic molecules [13–17]. As a result, there is currently a great interest in extending DFT to excited electronic states [18]. In this context, the time dependent DFT approach (TDDFT) offers an effective means to the calculation of vertical electronic excitation spectra of closed shell molecules.

In this paper, we have investigated the ground states of six metal complexes, namely $M(tpy)_2^{2+}$ (M = Fe (**1**), Ru (**2**), Os (**3**), tpy = terpyridine), $M(B\text{-}ptpy)_2^{2+}$ (M = Fe (**4**), Ru (**5**), Os (**6**), B = *n*-butyl, ptpy = phenylterpyridine, see Fig. 1) using DFT techniques, aiming at studying the effects of different metal atoms and the introduction of electron-donating substituents on the molecular geometry and electronic structure. TDDFT is used to find the characters, energies and oscillator strengths of singlet and triplet excited states of $M(tpy)_2^{2+}$ (M = Fe, Ru, Os). The results will be

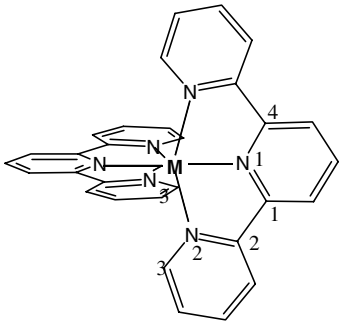

$M(tpy)_2^{2+}$ (M=Fe(**1**), Ru(**2**), Os(**3**))

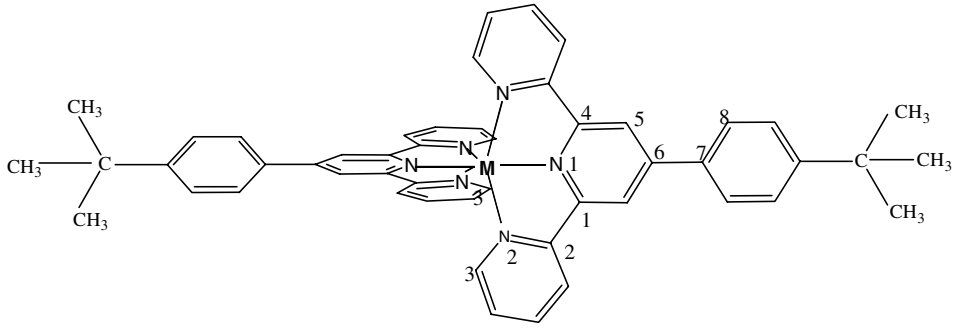

$M(B\text{-}ptpy)_2^{2+}$ (M=Fe(**4**), Ru(**5**), Os(**6**))

Fig. 1. Structures and atom labeling for metal compounds under study.

compared to the experimental studies of the photophysical properties of this class of complexes.

2. Computational methods

The electronic ground-state calculations of metal complexes have been performed using Becke's three-parameter hybrid exchange functional and Lee–Yang Parr correlation functional (B3LYP) with "Double-ζ" Lanl2DZ basis set for metal atoms and ligands, which uses Duning D95V basis set on first row atoms and Los Alamos ECP plus DZ on Na-Bi. Some reports showed Lanl2DZ basis set was successfully applied in some large systems including transition metal atoms, such as $M(phen)_3^{n+}$ (M = Co, Zn, Ru, Os) [19], $M(bpy)_3^{n+}$ (M = Re, Ru, Os) [20] and $M(tap)_3^{2+}$ (M = Fe, Ru, Os) [21]. The molecular geometries were full optimized without symmetry constraints. On the basis of the respective ground-state geometries, TDDFT calculations using the same functional have been carried out. The 10 lowest triplet and 40 singlet excited states of the closed shell complexes were calculated to obtain the vertical excitation energies for $M(tpy)_2^{2+}$ (M = Fe, Ru, Os). Unrestricted B3LYP calculations were performed for optimizing the lowest triplet state of $Ru(tpy)_2^{2+}$ and the luminescence properties of $Ru(tpy)_2^{2+}$ were obtained by TDDFT. To estimate the possible response of coordination energy due to the solvation, the solvent were modeled by the polarizable continuum model (PCM). All calculations were carried out with the GAUSSIAN98 software package [22].

3. Results and discussion

3.1. Molecular structure

The molecular structures under study are illustrated in Fig. 1 along with the numbering of some key atoms. The calculated results for $M(tpy)_2^{2+}$ (M = Fe (**1**), Ru (**2**), Os (**3**)) and $M(B\text{-}ptpy)_2^{2+}$ (M = Fe (**4**), Ru (**5**), Os (**6**)) and the available experimental data are summarized in Table 1. Table 1 lists the mean values of the computational and experimental bond lengths, angles and dihedral angles. Though there is no symmetrical constraint on the molecular structure, the optimized results show that the molecular symmetry basically belongs to D_{2d} point group and two ligands in every compound exhibit the nearly same geometrical parameters. The agreement between computed and experimental parameters is very good: the critical metal–nitrogen bonds are accurately reproduced, as well as N1–M–N2 bond angles. As shown in Table 1, the dihedral angle between two ligand planes for every molecule is approximately equal to 90°, which indicates the pseudo-octahedral structures for six compounds are maintained. Moreover, our optimized structures for $M(B\text{-}ptpy)_2^{2+}$ (M = Fe (**4**), Ru (**5**), Os (**6**)), respectively, show a twist angle of 28.7°, 29.5°, 29.6° of the phenyl and the pyridine rings, which are again in agreement with the theoretical result of 30° predicted by Amouyal et al. [12] for the similar structures. The calculated coordination bond lengths follow the order of Ru–N1 (0.2011 nm) > Os–N1 (0.2005 nm) > Fe–N1 (0.1913 nm) and Ru–N2 (0.2110 nm) > Os–N2 (0.2090 nm) > Fe–N2(0.2015 nm). The results show that the coordination bond lengths of second-row transition metal compound are the longest in the same group, and the similar results were also reported in [13] and [21]. For $Fe(tpy)_2^{2+}$, this result is reasonable because the number of outer shells of Fe^{2+} is smaller than that of Ru^{2+}. However, as the case of $Os(tpy)_2^{2+}$, this order is unexpected since the number of outer shells of Os^{2+} is larger than that of Ru^{2+} (Fe (3d) → Ru(4d) → Os(5d)). So in order to understand these results, the natural population analysis proposed by Löwdin [25] is applied to calculate the metal charge. The calculated metal charge is $+0.71|e^-|$ for Ru and $+1.01|e^-|$ for Os in $M(tpy)_2^{2+}$. The well-known cooperative effect was defined as follow:

Table 1
Main geometrical parameters (nm and degrees) of $M(tpy)_2^{2+}$ and $M(B\text{-}ptpy)_2^{2+}$ (M = Fe, Ru, Os)

Parameters	$Fe(tpy)_2^{2+}$		$Ru(tpy)_2^{2+}$		$Os(tpy)_2^{2+}$		$Fe(B\text{-}ptpy)_2^{2+}$	$Ru(B\text{-}ptpy)_2^{2+}$	$Os(B\text{-}ptpy)_2^{2+}$
	Calc.	Exp. [23]	Calc.	Exp. [24]	Calc.	Exp. [24]			
MN1	0.1913	0.1878	0.2011	0.1984	0.2005	0.1971	0.1910	0.2010	0.2006
MN2	0.2015	0.1981	0.2110	0.2074	0.2090	0.2060	0.2017	0.2110	0.2090
N1C1	0.1360		0.1360	0.1345	0.1370	0.1360	0.1362	0.1368	0.1376
N2C2	0.1380		0.1380	0.1374	0.1390	0.1385	0.1380	0.1387	0.1393
C1C2	0.1470		0.1470	0.1466	0.1470	0.1454	0.1480	0.1482	0.1476
N2C3	0.1350		0.1360	0.1350	0.1360	0.1325	0.1356	0.1359	0.1365
MN1C1	119.0		118.8	119.4	119.1	119.1	119.4	119.2	119.5
MN2C2	113.8		113.8	113.4	114.3	113.0	113.9	113.7	114.4
MN2C3	127.2		126.6	127.5	126.4	128.2	127.1	127.1	126.7
N1MN2	81.5	81.2	78.9	78.6	78.9	79.4	80.9	78.7	78.5
C1N1C4	122.2		122.6		121.8		121.1	121.6	121.0
C5C6C7C8							28.7	29.5	29.6
N1MN2N3	90.0		89.9	91.2	90.0	91.1	90.0	90.0	90.0

a donation from a σorbital of the ligand toward an empty d_σ orbital of the metal and a concurrent back-donation from a filled d_π orbital to a π* antibonding orbital of the ligand, and two processes promote and strengthen each other [26,27]. The substantial variations of metal charge from +0.71|e⁻| for Ru to +1.01|e⁻| for Os indicates a stronger back-donation to the π* antibonding orbital of the tpy ligand, which results in the shorter coordination bond length of Os–N than that of Ru–N. The introduction of electron-donating groups in $M(B\text{-ptpy})_2^{2+}$ (M = Fe (**4**), Ru (**5**), Os (**6**)) have little effect on the coordination bond lengths, as well as other bond lengths and angles.

3.2. Electronic structure

The energies of the eight highest occupied and eight lowest unoccupied molecular orbitals from the DFT/B3LYP calculation for the six complexes are listed in Table 2 and are schematically plotted in Fig. 2. For the six metal systems, the LUMO and LUMO + 1 are a set of quasi degenerate orbitals. As for $M(tpy)_2^{2+}$ (M = Fe, Ru, Os), the energy between the HOMO and quasi degenerate orbitals – HOMO − 1 and HOMO − 2 increases from 0.12 to 0.17 eV as the atomic number increases from Fe to Os. However, as the case of $M(B\text{-ptpy})_2^{2+}$ (M = Fe, Ru, Os), the HOMO and

Table 2
The energies (eV) of molecular orbitals of the metal complexes

	$Fe(tpy)_2^{2+}$	$Ru(tpy)_2^{2+}$	$Os(tpy)_2^{2+}$	$Fe(B\text{-ptpy})_2^{2+}$	$Ru(B\text{-ptpy})_2^{2+}$	$Os(B\text{-ptpy})_2^{2+}$
LUMO + 7	−6.62	−6.47	−6.41	−6.12	−6.00	−5.95
LUMO + 6	−6.62	−6.64	−6.73	−6.14	−6.18	−6.28
LUMO + 5	−6.63	−6.64	−6.73	−6.14	−6.18	−6.28
LUMO + 4	−6.67	−6.74	−6.84	−6.19	−6.28	−6.40
LUMO + 3	−7.65	−7.57	−7.55	−7.05	−7.00	−7.00
LUMO + 2	−7.68	−7.65	−7.71	−7.08	−7.09	−7.17
LUMO + 1	−7.83	−7.78	−7.82	−7.23	−7.22	−7.27
LUMO	−7.83	−7.78	−7.82	−7.24	−7.23	−7.28
HOMO	−11.51	−11.20	−10.96	−10.42	−10.26	−10.14
HOMO − 1	−11.63	−11.31	−11.13	−10.42	−10.26	−10.14
HOMO − 2	−11.63	−11.31	−11.13	−10.90	−10.64	−10.42
HOMO − 3	−12.39	−12.35	−12.37	−10.97	−10.88	−10.84
HOMO − 4	−12.44	−12.40	−12.43	−10.97	−10.89	−10.84
HOMO − 5	−13.19	−13.20	−13.26	−11.11	−10.93	−10.89
HOMO − 6	−13.19	−13.20	−13.26	−11.11	−10.94	−10.89
HOMO − 7	−13.59	−13.66	−13.74	−11.83	−11.82	−11.85

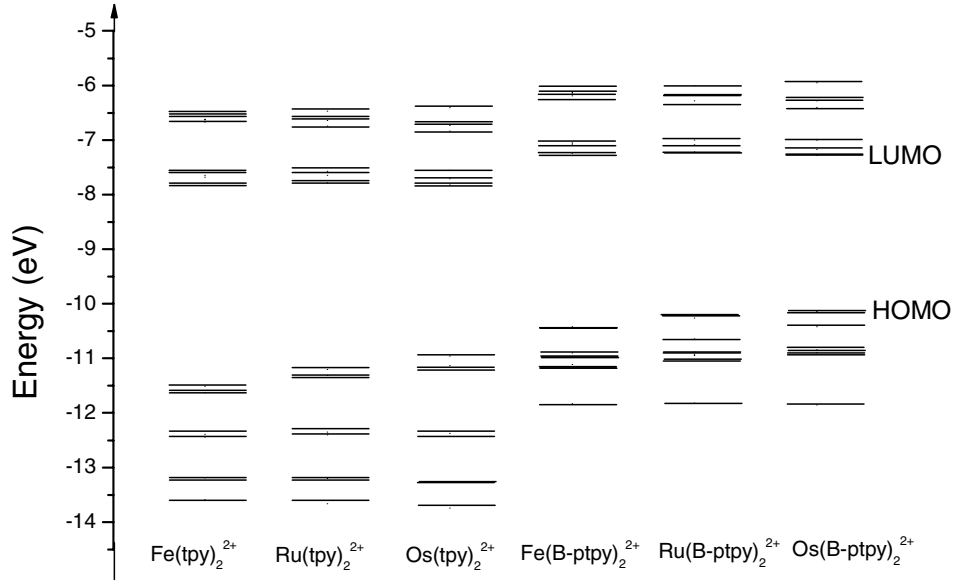

Fig. 2. Diagrams of energies of some frontier molecular orbitals in six compounds.

HOMO − 1 are quasi degenerate orbitals. The energy gap between the degenerate orbitals and HOMO − 2 decreases (0.48 eV (**4**) → 0.38 eV (**5**) → 0.28 eV (**6**)) as the number of the outer shells increase. When the contribution of the electronic transition from HOMO to LUMO to the lowest singlet (triplet) state $S_1(T_1)$ is dominant, the energy gap between HOMO and LUMO will be proportional to the vertical excitation energy of $S_0 \rightarrow S_1(T_1)$ and the transition energy of $S_1(T_1) \rightarrow S_0$. So the investigation on the trend of ΔE_{H-L} will give some useful information for the absorption or emission spectra. For two series of compounds $M(tpy)_2^{2+}$ and $M(B\text{-}ptpy)_2^{2+}$ (M = Fe, Ru, Os), the energy interval ΔE_{H-L} decreases gradually with the increase of the atomic number (3.68 eV (**1**) > 3.42 eV (**2**) > 3.14 eV (**3**) and 3.18 eV (**4**) > 3.03 eV (**5**) > 2.86 eV (**6**)). The introduction of donors in $M(B\text{-}ptpy)_2^{2+}$ results in a larger destabilization on the HOMO orbital than the LUMO orbital with respect to the corresponding $M(tpy)_2^{2+}$ (M = Fe, Ru, Os). The same result was predicted by Maestri et al. [28] for Ru complexes. The effect can be understood by considering that removal of one electron from the metal causes the formation of Ru^{3+} which withdraws electronic charge from the two B-ptpy ligands destabilizing the HOMO metal orbitals. For the same metal atom, the energy gap between HOMO and LUMO decreases with the addition of the electron-donating groups (3.68 eV (**1**) > 3.18 eV (**4**), 3.42 eV (**2**) > 3.03 eV (**5**), 3.14 eV (**3**) > 2.86 eV (**6**)).

Frontier orbitals play a relevant role in such system because they rule the redox reaction in which the dyes are involved during or after the electronic excitations. In order to study the molecular orbital components of HOMO and LUMO for six molecules, stereographs of the HOMO and LUMO orbitals of complexes **1**–**6** are shown in Fig. 3. For the DFT calculated orbitals, the HOMO of $Fe(tpy)_2^{2+}$ are mostly located on a single tpy ligand, whereas the LUMO is spread equally over the two tpy ligands. For $Ru(tpy)_2^{2+}$ and $Os(tpy)_2^{2+}$, the HOMO are mostly localized on the metal atom showing a clear $d_{x^2-y^2}$ shape, and the components of LUMO come mainly from two tpy ligands. The DFT calculations result in HOMOs and LUMOs consistent with the lowest energy transition assigned as MLCT for $Ru(tpy)_2^{2+}$ and $Os(tpy)_2^{2+}$ and intraligand (IL) transitions for $Fe(tpy)_2^{2+}$. As is the case of $M(B\text{-}ptpy)_2^{2+}$ (M = Fe, Ru, Os), the HOMO and LUMO have the similar features and the competents of HOMO and LUMO become more complicated compared with $M(tpy)_2^{2+}$. As expected, the HOMO has a strong d-metal character, but significant contributions come from the phenyl π orbitals, while the LUMOs are mainly localized on a single tpy ligand and little partly d orbitals of metal atoms. Consequently, the lowest energy transitions in ground states of $M(B\text{-}ptpy)_2^{2+}$ (M = Fe, Ru, Os) should be assigned as mixed metal/ligand-to-ligand charge transfer. As can be seen in Fig. 3, the introduction of donors in metal systems importantly changes the character of lowest energy transitions, which also was observed in [28].

3.3. Coordination energy

The coordination energy ΔE can be applied to study the stabilities of metal complexes, which is defined as

$$\Delta E = 2E_{\text{ligand}} + E_{\text{M}}^{2+} - E_{\text{comp}} \quad (1)$$

for the process

$$M^{2+} + 2\text{ligand} \rightarrow M(\text{ligand})_2^{2+}. \quad (2)$$

Here E_{ligand}, E_{M}^{2+} and E_{comp} are the energies of ligand, metal ion and the metal complex, respectively. The B3LYP/Lanl2DZ method is carried out on the metal ion and ligand. The calculated coordination energies are listed in Table 3. The definition suggests the larger the positive value of ΔE is, the more stable the complex is. As shown in Table 3, in vacuo, the ΔE value is 23.83 eV for **1**, 24.21 eV for **2**, 26.61 eV for **3** and 24.38 eV for **4**, 24.72 eV for **5**, 27.12 eV for **6**, respectively. The results indicate with the increase of atomic number in the metal atom, the metal compound becomes more chemically stable. The introduction of electron-donating substituents also has a positive effect on the chemical stability for the same metal ion. In order to explore the influence of solvation effects on the coordination energies, we calculated ΔE values of $M(tpy)_2^{2+}$ (M = Fe, Ru, Os) in ethanol. The results in Table 3 indicate that inclusion of solvation effects leads to a decrease of absolute values of ΔE, but does not change the trend of chemical stability from Fe to Ru and to Os.

3.4. Excitation energies

Time dependent density functional calculations are employed to examine the low-lying singlet and triplet excited states of $M(tpy)_2^{2+}$ (M = Fe, Ru, Os) on the basis of the ground-state geometries. The vertical electronic excitation energies, oscillator strength, the most significant transitions contributing to each excited state and the assignment of the character of each excited state are shown in Tables 4–6. For $Ru(tpy)_2^{2+}$, 40 excited states were considered in order to depict the visible and UV absorptions exhibited by this chromophore. Only six lowest excited states and only those higher energy states which contribute to the observed absorption spectrum are given in Table 5. To independently check these calculations produce reasonable results, the absorption spectrum of $Ru(tpy)_2^{2+}$ has been stimulated based on the TDDFT calculations and is shown in Fig. 4. For $Fe(tpy)_2^{2+}$ and $Os(tpy)_2^{2+}$, five lowest singlet excited states are listed in Tables 4 and 6.

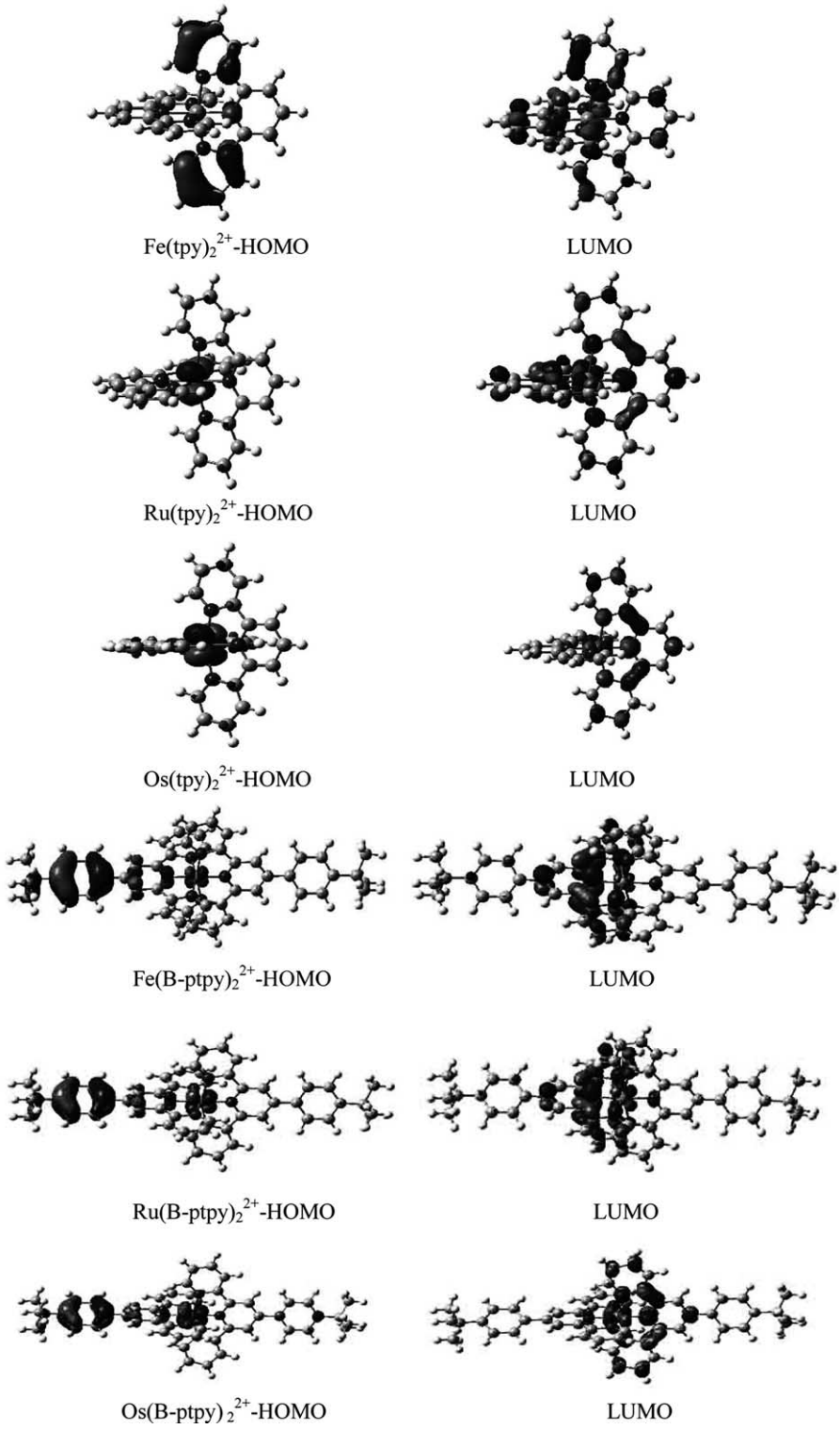

Fig. 3. Contour plots of HOMO and LUMO in six metal compounds.

An experimentally used model of an excited state corresponds to excitation of an electron from an occupied to a virtual molecular orbital. However, the excited states calculated herein demonstrate that excited-state electronic structures are best described in terms of multi-configurations, wherein a linear combination of several occupied-to-virtual molecular orbital excitations comprises a given optical transition. Assignment of the character of each excited state was based on the compositions of the occupied and

Table 3
Compound coordination energies (ΔE/eV) for $M(tpy)_2^{2+}$ in vacuo and ethanol and $M(B\text{-}ptpy)_2^{2+}$ in vacuo

Compound	E_M^{2+}	E_{ligand}	$E_{comp.}$	ΔE
In vacuo				
$Fe(tpy)_2^{2+}$	−3329.00	−20199.38	−43751.59	23.83
$Ru(tpy)_2^{2+}$	−2524.40	−20199.38	−42947.37	24.21
$Os(tpy)_2^{2+}$	−2445.10	−20199.38	−42870.47	26.61
$Fe(B\text{-}ptpy)_2^{2+}$	−3329.00	−30764.08	−64881.54	24.38
$Ru(B\text{-}ptpy)_2^{2+}$	−2524.40	−30764.08	−64077.30	24.74
$Os(B\text{-}ptpy)_2^{2+}$	−2445.10	−30764.08	−64000.38	27.12
In ethanol				
$Fe(tpy)_2^{2+}$	−3348.39	−20200.24	−43757.02	8.15
$Ru(tpy)_2^{2+}$	−2544.01	−20200.24	−42952.79	8.30
$Os(tpy)_2^{2+}$	−2464.02	−20200.24	−42875.88	11.38

Table 4
Selected TDDFT calculated energies and compositions of the lowest lying singlet and triplet energy states together with oscillator of $Fe(tpy)_2^{2+}$

	Energy (eV nm)	f	Composition	Character
S1	2.582 (480.0)	0.0114	E(1) HOMO → LUMO, 33% HOMO − 1 → LUMO + 10, 11% E(2) HOMO → LUMO + 1, 33% HOMO − 2 → LUMO + 10, 11%	tpy(π) → tpy(π*)
S2	2.704 (458.3)	0.0014	E(1) HOMO − 2 → LUMO + 11, 20% HOMO → LUMO, 12% E(2) HOMO − 1 → LUMO + 11, 20% HOMO → LUMO + 1, 12%	tpy(π) → tpy(π*)
S3	2.712 (457.1)	0.0000	HOMO − 2 → LUMO, 25% HOMO − 1 → LUMO + 1, 25%	tpy(π) → tpy(π*)
S4	2.719 (455.8)	0.0000	HOMO − 2 → LUMO + 1, 25% HOMO − 1 → LUMO, 25%	tpy(π) → tpy(π*)
S5	2.884 (429.8)	0.0530	HOMO − 2 → LUMO + 1, 23% HOMO − 1 → LUMO, 23%	tpy(π) → tpy(π*)

virtual molecular orbitals of the dominant configuration(s) for that excited state. As for the lowest singlet excited state S_1 of $M(tpy)_2^{2+}$ (M = Fe, Ru, Os), it is degenerate state as shown in Tables 4–6. For $Fe(tpy)_2^{2+}$, since the occupied orbitals (HOMO − 2, HOMO − 1 and HOMO) mostly come from terpyridine π and the virtual orbitals (LUMO, LUMO + 1 and LUMO + 10) are constituted importantly by terpyridine π*, the transition is designated a IL transition. Whereas for S_1 of $Ru(tpy)_2^{2+}$ and $Os(tpy)_2^{2+}$, the dominant excitation is from HOMO having a metal d orbital character to LUMO and LUMO + 1 with terpyridine π* character and has been termed a MLCT.

From Tables 4–6, it can be seen that consistent with the variation rules of the energy gaps, with the increasing the atomic number the absorption bands exhibit red-shifts: for S_1, 480.0 nm (**1**) < 500.7 nm (**2**) < 557.0 nm (**3**). This variation is consistent with the decrease of electron density on the metal resulting in a destabilization of its partially filled d orbitals and the order of bearing a positive charge is Fe < Ru < Os.

The 10 lowest triplet excited states of $Ru(tpy)_2^{2+}$ were also calculated using analogous TDDFT methodology. The first four triplet excited states are shown in Table 5. As expected from Hund's rule, transitions to the triplet states tend to be lower in energy than their corresponding singlets. As can be seen from Table 5, the first triplet vertical transition energy of $Ru(tpy)_2^{2+}$ is 0.239 eV lower than that of the first singlet excited state (2.136 vs. 2.475 eV). Because singlet → triplet transitions are formally spin forbidden, all have zero oscillator strength since singlet–triplet mixing was not taken into account in these calculations. These triplet excited states correspond to the "triplet state absorption", which can not be observed experimentally. It is thus not possible from our results to determine what effect these triplet states have on the ground-state absorption spectrum of $Ru(tpy)_2^{2+}$.

3.5. Comparison with experimental results

Among the $M(tpy)_2^{2+}$ type complexes, $Ru(tpy)_2^{2+}$ was the most extensively investigated since it is capable of playing the role of photosensitizers in

Table 5
Selected TDDFT calculated energies and compositions of the lowest lying singlet and triplet energy states together with oscillator of $Ru(tpy)_2^{2+}$ and the experimental results

	Energy eV (nm)	f	Composition	Character	Exp. [12] (nm) (ε_{max} (M^{-1} cm^{-1}))
Singlet					
S1	2.475 (500.7)	0.0206	E(1) HOMO → LUMO, 47% E(2) HOMO → LUMO + 1, 47%	Ru(d) → tpy(π*)	
S2	2.518 (492.3)	0.0000	HOMO − 1 → LUMO, 24% HOMO − 2 → LUMO + 1, 24%	Ru(d) → tpy(π*)	
S3	2.591 (478.4)	0.0000	HOMO − 1 → LUMO + 1, 25% HOMO − 2 → LUMO, 25%	Ru(d) → tpy(π*)	
S4	**2.742 (452.1)**	**0.0273**	**HOMO − 1 → LUMO, 16%** **HOMO − 2 → LUMO + 1, 16%** **HOMO → LUMO + 2, 16%**	**Ru(d) → tpy(π*)**	**473 (16 100)**
S5	2.776 (446.5)	0.0000	HOMO → LUMO + 3, 27% HOMO − 1 → LUMO + 1, 10% HOMO − 2 → LUMO, 10%	Ru(d) → tpy(π*)	
S6	2.916 (425.1)	0.0178	E(1) HOMO − 1 → LUMO + 2, 46% E(2) HOMO − 2 → LUMO + 2, 46%	Ru(d) → tpy(π*)	
S19	4.029 (307.7)	0.0474	E(1) HOMO − 3 → LUMO, 31% HOMO − 4 → LUMO + 1, 12% E(2) HOMO − 3 → LUMO + 1, 31% HOMO − 4 → LUMO, 12%	tpy(π) → tpy(π*)	
S20	**4.136 (299.7)**	**0.8200**	**E(1) HOMO − 4 → LUMO, 26%** **HOMO → LUMO + 6, 10%** **E(2) HOMO − 4 → LUMO + 1, 26%** **HOMO → LUMO + 5, 10%**	**tpy(π) → tpy(π*)** **Ru(d) → tpy(π*)**	**306 (72 300)**
S24	4.445 (278.8)	0.0244	E(1) HOMO − 2 → LUMO + 12, 33% HOMO − 1 → LUMO + 10, 8% E(2) HOMO − 1 → LUMO + 12, 33% HOMO − 2 → LUMO + 10, 8%	Ru(d) → tpy(π*)	
S25	**4.481 (276.6)**	**0.1336**	**HOMO − 3 → LUMO + 3, 21%** **HOMO − 4 → LUMO + 2, 14%**	**tpy(π) → tpy(π*)**	**270 (48 000)**
S27	4.629 (267.8)	0.0192	E(1) HOMO → LUMO + 8, 46% E(2) HOMO → LUMO + 9, 46%	Ru(d) → tpy(π*)	
Triplet					
T1	2.136 (580.3)	0.0000	HOMO − 2 → LUMO, 29% HOMO − 1 → LUMO + 1, 29%	Ru(d) → tpy(π*)	
T2	2.201 (563.2)	0.0000	HOMO − 2 → LUMO + 1, 27% HOMO − 1 → LUMO, 27%	Ru(d) → tpy(π*)	
T3	2.279 (543.9)	0.0000	E(1) HOMO → LUMO, 51% E(2) HOMO → LUMO + 1, 51%	Ru(d) → tpy(π*)	
T4	2.413 (513.7)	0.0000	HOMO − 2 → LUMO, 27% HOMO − 1 → LUMO + 1, 27%	Ru(d) → tpy(π*)	

Table 6
Selected TDDFT calculated energies and compositions of the lowest lying singlet and triplet energy states together with oscillator of $Os(tpy)_2^{2+}$

	Energy (eV nm)	f	Composition	Character
S1	2.226 (557.0)	0.0288	E(1) HOMO → LUMO, 47% E(2) HOMO → LUMO + 1, 47%	Os(d) → tpy(π*)
S2	2.299 (539.3)	0.0000	HOMO − 2 → LUMO + 1, 24% HOMO − 1 → LUMO, 24%	Os(d) → tpy(π*)
S3	2.399 (516.7)	0.0000	HOMO − 2 → LUMO, 25% HOMO − 1 → LUMO + 1, 25%	Os(d) → tpy(π*)
S4	2.510 (493.8)	0.0028	HOMO → LUMO + 2, 28% HOMO − 2 → LUMO + 1, 10% HOMO − 1 → LUMO, 10%	Os(d) → tpy(π*)
S5	2.586 (479.3)	0.0000	HOMO → LUMO + 3, 28% HOMO − 2 → LUMO, 10% HOMO − 1 → LUMO + 1, 10%	Os(d) → tpy(π*)

covalently-linked multicomponent systems. The experimental results indicate that the very intense bands centered at 306 nm in the UV region can be assigned to ligand-centered π–π* transitions. The relatively intense and broad absorption band around 473 nm in the visible region which is responsible for the deep

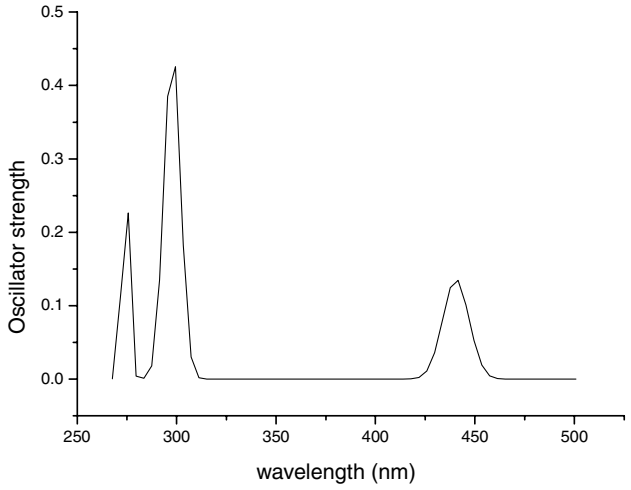

Fig. 4. Calculated electronic absorption spectrum of the $Ru(tpy)_2^{2+}$ complex.

red color, is owing to a spin-allowed $d \rightarrow \pi^*$ MLCT transition [12].

The TDDFT calculation shows that the lowest singlet states S_1 is a degenerate state and presents the excitation energy 2.475 eV (500.7 nm). It corresponds to excitations from an electron in nondegenerate HOMO with significant 5d character to the lowest π^* orbitals of the terpyridine ligands, i.e., MLCT transition. The S_4 state vertical excitation energy lies 0.267 eV above the maximum of the $S_0 \rightarrow S_1$ transition, which belongs to the MLCT state given the strong 5d component of the occupied orbitals and the predominantly ligand π^* virtual orbital. Similarly, the degenerate S_6 state is also assigned as MLCT transition. We assign the S_1, S_4 and S_6 states as those responsible for the experimentally weak absorption structure with the character of MLCT around 473 nm [12]. As shown in Fig. 4 and Table 5, there are excited states having significant oscillator strength throughout the 4–4.6 eV region, but the strongest are clustered around 4.13 eV (299.7 nm) and 4.48 eV (276.6 nm) (referred as to the second and third bands in Fig. 4, respectively). Both these bands are approximately an order of magnitude more intense than the low energy MLCT band. We can ascribe the band at 299.7 nm to the $S_0 \rightarrow S_{20}$ with the oscillator strength of 0.82 and the band at 276.6 nm to the $S_0 \rightarrow S_{25}$ with the oscillator strength of 0.13. These are in good agreement with the experimentally observed two bands around 306 and 270 nm [12]. As can be seen from Table 5, only the S_{25} is a pure IL π–π^* state, while the S_{20} states are of strongly mixed MLCT and IL characters. But for S_{20} state, it can be roughly described as having IL character 2.5 times as MLCT character. So S_{20} state can be assigned as IL states.

3.6. Lowest triplet state and emissive spectrum of $Ru(tpy)_2^{2+}$

Unrestricted B3LYP calculations were considered to optimize the lowest triplet state T_1 of $Ru(tpy)_2^{2+}$. The geometrical parameters are collected in Table 7 with those of the ground state. From Table 7, one can find that the geometrical parameters for excited state T_1 have some differences from those of the ground state. The Ru–N1 bond distance in the triplet state is obviously shorter than that in the ground state by 0.05 nm, and there is basically no change in the distance of Ru–N2 (0.2110–0.2118 nm). The distances between the nitrogen atom and carbon atom in the triplet states are lengthened with respect to those in the ground state. The change of bond angles is small (~1°). In general, all the geometrical variations are consistent with the occupation of the π^* orbitals of the terpyridine ligands depicted in Fig. 3 and the variation path follows the bonding–antibonding scheme in such plots.

In rigid matrix at 77 K, $Ru(tpy)_2^{2+}$ exhibit a strong long-lived luminescence characteristic of a triplet MLCT (^{3}MLCT) level. From the maximum of the luminescence band, the energy of the lowest excited state results to be 2.07 eV. On increasing temperature, the $Ru(tpy)_2^{2+}$ luminescence intensity and lifetime decrease. At room temperature, $Ru(tpy)_2^{2+}$ is practically not luminescent [8].

Based on the excited triplet state geometry of $Ru(tpy)_2^{2+}$, TDDFT is used to calculate the emission spectra. The calculated lowest triplet state T_1 corresponding to the photoluminescence for $Ru(tpy)_2^{2+}$, consists of the transition from HOMO to LUMO and thus is assigned as MLCT. The calculated emissive wavelength is 688.6 nm, which is longer than the experimental result – 598.9 nm. Concerning the reasons for such deviations, we want to stress several points. First, TDDFT systematically underestimated the excitation energies by 0.4–0.7 eV comparing to the experimental results [29,30] due to the limitation of the current approximate exchange-correlation functionals in cor-

Table 7
Main geometrical parameters (nm and degrees) of the ground state and the lowest triplet state of the $Ru(tpy)_2^{2+}$ compound

Parameters	S_0	T_1
MN1	0.2011	0.1962
MN2	0.2110	0.2118
N1C1	0.1360	0.1413
N2C2	0.1380	0.1398
C1C2	0.1470	0.1457
N2C3	0.1360	0.1362
MN1C1	118.8	118.6
MN2C2	113.8	112.7
MN2C3	126.6	127.8
N1MN2	78.9	79.8
C1N1C4	122.6	122.8
N1MN2N3	89.9	90.1

rectly describing the exchange-correlation potential in the asymptotic region [31,32]. Especially, the more detailed interpretation of phosphorescence properties will await the inclusion of spin–orbit coupling effects, which are not included in these TDDFT results. Second is the solvent effect. Usually the studied system is put in a gas-phase environment for the quantum method, whereas it is laid in a solution environment in experiment, and our limited studies did not take the solvent effects into account and thus did not add an effects rectification. We hope to investigate these effects in future studies.

4. Conclusion

We have applied DFT method to study some important trends in electronic structures and ground- and excited-state properties of complexes $M(tpy)_2^{2+}$ and $M(B\text{-}ptpy)_2^{2+}$ (M = Fe, Ru, Os). The results indicate that for each series of compound, with the increase the numbering of the outer shell, the energy gap between HOMO and LUMO decreases and the chemical stability of complex increases. As for the same metal ion, the introduction of donors in complex causes the decrease of the energy interval between HOMO and LUMO and the increase of the chemical stability. Excited singlet and triplet states are examined using TDDFT method. The results show that, for $Ru(tpy)_2^{2+}$ and $Os(tpy)_2^{2+}$, the lowest energy transition are assigned as the singlet MLCT. For $Fe(tpy)_2^{2+}$, the lowest energy transition corresponds to the IL π–π^* character. The calculated absorption and emission spectra of $Ru(tpy)_2^{2+}$ well reproduce the experimental observation.

Acknowledgements

This work is supported by the Major State Basis Research Development Program (No. 2002CB 613406) and the National Nature Science Foundation of China (No. 90101026) and the Key Laboratory for Supramolecular Structure and Material of Jilin University.

References

[1] V. Balzani, A. Juris, M. Venturi, S. Campagna, S. Serroni, Chem. Rev. 96 (1996) 956.
[2] F. Barigelletti, L. Flamigni, Chem. Soc. Rev. 29 (2000) 1.
[3] L. Sun, L. Hammarström, B. Åkermark, S. Styring, Chem. Soc. Rev. 30 (2001) 36.
[4] R. Ballardini, V. Balzani, A. Credi, M.T. Gandolfi, M. Venturi, Acc. Chem. Res. 34 (2001) 445.
[5] D. Pomeranc, V. Heitz, J.-C. Chambron, J.-P. Sauvage, J. Am. Chem. Soc. 123 (2001) 12215.
[6] A. Juns, V. Balzani, F. Barigelletti, S. Campagna, P. Belser, A. von Zelewsky, Coord. Chem. Rev. 84 (1988) 85.
[7] M.K.De Armond, L.M. Myrick, Acc. Chem. Res. 22 (1989) 364.
[8] J.-P. Sauvage, J.-P. Collin, J.-C. Chambron, S. Guillerez, C. Coudret, Chem. Rev. 94 (1994) 993.
[9] M.L. Stone, A.G. Crosby, Chem. Phys. Lett. 79 (1981) 169.
[10] E.M. Kober, J.L. Marshall, W.L. Dressick, B.P. Sullivan, J.-V. Caspar, J.T. Meyer, Inorg. Chem. 24 (1985) 2755.
[11] C. Creutz, M. Chou, T.L. Netzel, M. Okumra, N. Sutin, J. Am. Chem. Soc. 102 (1980) 1309.
[12] E. Amouyal, M. Mouallem-Bahout, G. Calzaferri, J. Phys. Chem. 95 (1991) 7641.
[13] J.-F. Guillemoles, V. Barone, L. Joubert, C. Adamo, J. Phys. Chem. A 106 (2002) 11354.
[14] P.J. Hay, J. Phys. Chem. A 106 (2002) 1634.
[15] M.Z. Zgierski, J. Chem. Phys. 118 (2003) 4045.
[16] S. Fantacci, F. De Angelis, A. Selloni, J. Am. Chem. Soc. 125 (2003) 4381.
[17] C. Makedonas, C.A. Mitsopoulou, F.J. Lahoz, A.I. Balana, Inorg. Chem. 42 (2003) 8853.
[18] E. Runge, E.K.U. Gross, Phys. Rev. Lett. 76 (1996) 1212.
[19] K.C. Zheng, X.W. Liu, H. Deng, H. Chao, F.C. Yun, L.N. Ji, J. Mol. Struct. (Theochem) 626 (2003) 295.
[20] K.C. Zheng, J.P. Wang, Y. Shen, D.B. Kuang, F.C. Yun, J. Phys. Chem. A 105 (2001) 7248.
[21] K.C. Zheng, J.P. Wang, Y. Shen, Y.W.L. Peng, F.C. Yun, J. Chem. Soc., Dalton Trans. (2002) 111.
[22] M.J. Frisch, G.W. Trucks, H.B. Schlegel, G.E. Scuseria, M.A. Robb, J.R. Cheeseman, V.G. Zakrzewski, J.A. Montgomery Jr., R.E. Stratmann, J.C. Burant, S. Dapprich, J.M. Millam, A.D. Daniels, K.N. Kudin, M.C. Strain, O. Farkas, J. Tomasi, V. Barone, M. Cossi, R. Cammi, B. Mennucci, C. Pomelli, C. Adamo, S. Clifford, J. Ochterski, G.A. Petersson, P.Y. Ayala, Q. Cui, K. Morokuma, N. Rega, P. Salvador, J.J. Dannenberg, D.K. Malick, A.D. Rabuck, K. Raghavachari, J.B. Foresman, J. Cioslowski, J.V. Ortiz, A.G. Baboul, B.B. Stefanov, G. Liu, A. Liashenko, P. Piskorz, I. Komaromi, R. Gomperts, R.L. Martin, D.J. Fox, T. Keith, M.A. Al-Laham, C.Y. Peng, A. Nanayakkara, M. Challacombe, P.M.W. Gill, B. Johnson, W. Chen, M.W. Wong, J.L. Andres, C. Gonzalez, M. Head-Gordon, E.S. Replogle, J.A. Pople, GAUSSIAN 98, Revision A.9, Gaussian, Inc., Pittsburgh PA, 1998.
[23] P. Lainé, A. Gourdon, J.-P. Launay, Inorg. Chem. 34 (1995) 5156.
[24] D.C. Craig, M.L. Scudder, W.-A. McHale, H.A. Goodwin, Aust. J. Chem. 51 (1998) 1131.
[25] R.-D. Löwdin, Phys. Rev. 97 (1955) 1474.
[26] M.J.S. Dewar, Bull. Soc. Chim. Fr. 18 (1951) C71.
[27] J. Chatt, L.A. Duncanson, J. Chem. Soc. (1953) 2939.
[28] M. Maestri, N. Armaroli, V. Balzani, E.C. Constable, A.M.W. Cargill Thompson, Inorg. Chem. 34 (1995) 2759.
[29] C. Hsu, S. Hirata, H. Martin, J. Phys. Chem. A 105 (2001) 451.
[30] Z. Cai, K. Sendt, J.R. Reimers, J. Chem. Phys. 117 (2002) 5543.
[31] D.J. Tozer, N.C. Handy, J. Chem. Phys. 109 (1998) 10180.
[32] M.E. Casida, C. Jamorski, K.C. Casida, D.R. Salahub, J. Chem. Phys. 108 (1998) 4439.